Engineering Science and Technology, an International Journal 17 (2014) 173–184

HOSTED BY

Contents lists available at ScienceDirect

Engineering Science and Technology, an International Journal

journal homepage: http://www.elsevier.com/locate/jestch

Full length article

Investigation of surface integrity, material removal rate and wire wear ratio for WEDM of Nimonic 80A alloy using GRA and Taguchi method

Amitesh Goswami*, Jatinder Kumar

Department of Mechanical Engineering, National Institute of Technology, Kurukshetra 136 119, Haryana, India

ARTICLE INFO

Article history:
Received 20 March 2014
Received in revised form
7 May 2014
Accepted 14 May 2014
Available online 14 June 2014

Keywords:
GRA
Material removal rate
Surface integrity
Taguchi
WEDM
Wire wear ratio

ABSTRACT

This paper presents the investigation on surface integrity, material removal rate and wire wear ratio of Nimonic 80A using WEDM process. Taguchi's design of experiments methodology has been used for planning and designing the experiments. All of the input parameters and two factors interactions have been found to be statically significant for their effects on the response of interest. SEM was performed on the machined samples to investigate the effect and microstructure of the samples after machining. A higher pulse-on time setting leads to thicker recast layer. At lower value of pulse-on time and higher value of pulse-off time, the wire deposition on the machined surface is low.

1. Introduction

Recent developments in mechanical industry have fuelled the demand for materials having high toughness, hardness and impact resistance. These materials are difficult to machine with traditional methods. The search for new, lightweight material with greater strength and toughness has led to the development of new generation of materials. Sometimes their properties may create major challenges during machining operations. Wire Electrical discharge machining (WEDM) has evolved from a simple means of making tools and dies to the best alternative of producing micro-scale parts with the highest degree of dimensional accuracy and surface finish quality. WEDM is a nontraditional, thermoelectric process which erodes material from the workpiece using a series of discrete sparks between a work and tool electrode separated by a thin film of dielectric fluid (deionised water). The dielectric is fed continuously to the machining area to flush away the eroded particles [12]. In WEDM cutting, a single-stranded thin wire electrode is fed continuously against the workpiece material through a CNC-controlled guidance system. Fig. 1 [5] shows the schematic representation of the WEDM. Sparks are formed through a sequence of rapid electrical pulses generated by the machine's power supply, thousands of times per second. Each spark forms an ionization channel under extremely high heat and pressure, in which particles flow between the wire electrode and the workpiece, resulting in vaporization of localized sections. The workpiece and the wire are always separated by a controlled gap, which is maintained constantly by the machine [19]. The used wire is collected at the bottom after use and the same cannot be reused again due to dimensional inaccuracies [18]. At the same time, the dielectric cutting fluid cools the material and flushes away particles that have been eroded from it [1]. Nimonic alloys are extensively used for the manufacturing of aeroengine components because of its high specific strength (strength to weight ratio), which is maintained at higher temperature [3]. During prolonged exposure to high temperatures, many metals begin to crack, deform, corrode, fatigue, etc. Nimonic alloys are used for their resistance to corrosion and retention of other mechanical properties at temperatures as high as 1100 °F, depending on the grade [2]. Hard abrasive carbides in the alloy results in high abrasive wear of the cutting tool. Presence of hard abrasive carbides in the microstructure and built up edges produced during machining results in poor machinability. Welding/adhesion of the alloy on the tool during machining, causes severe notching and spalling on the tool face due to the consequent pull-out of the tool material [2,4]. Normal stresses on the tool are

* Corresponding author.
E-mail addresses: amitesh550@yahoo.com (A. Goswami), jatin.tiet@gmail.com (J. Kumar).
Peer review under responsibility of Karabuk University.

http://dx.doi.org/10.1016/j.jestch.2014.05.002

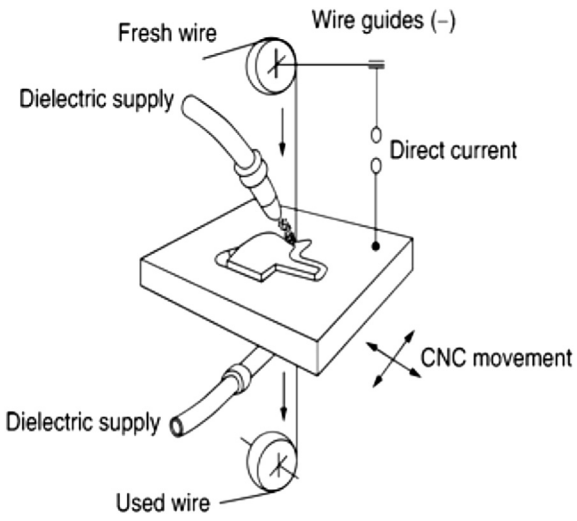

Fig. 1. Schematic representation of the WEDM [5].

roughly twice as high for machining nimonic alloy as for machining steel under the same cutting parameters. This result in breakdown of the cutting tool because of higher stresses applied behind the cutting edge [4]. High temperature is generated at the tool tip due to the poor thermal diffusivity of the Nimonic alloy resulting in tool wear. During machining, high strength is maintained at elevated temperatures, which opposes the plastic deformation needed for chip formation. Production of a tough and continuous chip contributes to the degradation of the cutting by seizure and cratering [3].

A comprehensive literature review has been performed on various aspects of WEDM process and has been summarized in Table 1. It is evident from the literature review; almost no investigation has been performed on the machinability of Nimonic 80A using WEDM process. Moreover the investigations reported on WEDM of the other conventional materials (listed in Table 1) have been focused on parametric optimization of WEDM process with MRR, surface roughness and dimensional deviation as the responses of interest. Very few studies have been reported on investigation of wire wear ratio [20,16]. Also the surface integrity aspects such as surface topography, recast layer and material migration among the electrodes have not been properly investigated in most of the reported studies (Table 1). Hence present study is targeted at investigation of machining characteristics (MRR, WWR) in WEDM of Nimonic 80A alloy along with the surface integrity aspects (surface topography, recast layer and material migration/EDS). The outcome of this study would add to scares database of the machinability of Nimonic 80A alloy and also would be extremely useful for the machinist as the technology charts for WEDM of Nimonic 80A alloy are not easily available.

2. Methodology

The experimental design proposed by Taguchi involves using orthogonal arrays to organize the parameters affecting the process and the levels at which they should be varied. The Taguchi method tests pairs of combinations instead of testing all possible combinations. This allows determining the major factors affecting the output, with a minimum amount of experimentation. Analysis of variance on the collected data from the experiments can be used to select new parameter values to optimize the performance characteristic [17]. A cause and effect diagram (Fig. 2) for identifying the potential factors that may affect the machining characteristics (such as MRR) was constructed. From the available literature on WEDM, total six numbers of input parameters were finally selected. In this work, L_{27} orthogonal array with six control factors viz., A, B, C, D, E, F and three interactions viz. A × B, A × C and B × C have been studied. The allocation of columns to the input parameters and interactions in the orthogonal array was done using linear graph. Signal to noise ratio was obtained using Minitab 16 software. Higher is better (HB) for MRR and lower is better (LB) for WWR were taken for obtaining optimum machining characteristics.

3. Experimentation

Experiments were performed on Electronica Sprintcut (Electra-Elplus 40A DLX) CNC wire electrical discharge machine to study the material removal rate and wire wear ratio affected by machining process variable at different setting of pulse-on time (T_{on}), pulse-off time (T_{off}), spark gap set voltage (SV) peak current (IP), wire feed (WF) and wire tension (WT). L_{27} orthogonal array (three levels) with six input variables was selected for experimentation. Fig. 3 shows the experimental setup of the WEDM. Tables 2 and 3 show the various process parameters with their values at three levels and L_{27} orthogonal array (with six input variables and three interactions assigned to different columns) respectively. Nimonic 80A (77.05% Ni, 18.39% Cr, 1.92% Ti, 1.05% Al, 0.63% Fe, 0.2% Mn, 0.19% Si) block of thickness 25 mm was used as work material. Specimens (Rectangular) of size 8 mm × 8 mm × 25 mm were prepared from the block using brass wire electrode of diameter 0.25 mm (Soft). De-ionized water was used as the dielectric fluid. The total length of each specimen was taken as 34.48 mm {32 + 1.84 + (0.16 × 4)} mm. In this 1.84 mm was the free straight cut and 0.16 mm was taken as left offset on all four sides. Digital stopwatch was used for precise calculation of the time taken (in minutes and seconds). Experiments were conducted thrice to minimize the chances of error. Material removal rate (MRR) was calculated by using the formula:

$$\text{Material removal rate(MRR)} = K \cdot \rho \cdot t \cdot \text{CR} \ \ \text{g/min.} \quad (1)$$

where, K is the kerf (mm), ρ is the density (0.00819 g/mm^3) of the material, t is the thickness (25 mm) of the workpiece and CR is the cutting rate (mm/min).

Wire wear ratio was calculated by using the formula:

$$\text{Wire wear ratio(WWR)} = (\text{IWW} - \text{FWW})/\text{IWW} \quad (2)$$

where,

IWW = initial weight of the wire
FWW = final weight of the wire after machining

Mitutoyo BH.V507 Coordinate Measuring Machine (Fig. 4a) and Mitutoyo digital outside micrometer were used for kerf (Fig. 4b) measurement. Fig. 4c shows the Machining profile of the workpiece. An electronic balance with 0.01 g accuracy was used to measure the weight. In order to minimize the measurement error the average value of three-weight measurements were used. Table 4 shows the various results of the material removal rate and Wire wear ratio, as per designed L_{27} orthogonal array. Minitab 16 software was used for ANOVA. Tables 5 and 6 shows the analysis of variance and F test for material removal rate and Wire wear ratio respectively.

4. Single response optimisation

The Taguchi approach for predicting the mean performance characteristics and determination of confidence intervals for the

Table 1
Literature review (tabular form).

Sr. No.	Investigator	material used	Experimental design technique	Input parameters considered	Output (response)	Findings of the study
1	[15]	Non-alloyed steel, wire electrodes of magnesium, tin and zinc	–	Pulse time, discharge time, open circuit voltage	Influence of wire electrode materials on machinability of WEDM	Cutting efficiency depends upon both melting temperature and work function. Cutting speed was observed to increase with the increase of the melting temperature and/or the decrease of the work function of the cathode material.
2	[11]	D2 tool steel	Taguchi's L_{27} orthogonal array, Non-linear regression analysis	Discharge current, Pulse duration, Pulse frequency, wire feed, wire tension, Dielectric flow rate	MRR, Surface roughness, kerf width	Discharge current, pulse duration, dielectric flow rate and the interaction between discharge current and pulse duration are most significant parameters for cutting operation.
3	[6]	SKDI1 alloy steel	Taguchi's L_{18} mixed orthogonal array, GRA	Table feed rate, pulse-on time, pulse-off time, Wire velocity, wire tension fluid pressure	MRR, surface roughness, gap width	Table feed rate and pulse-on time have main influence on the MRR and pulse-on time have significant influence on the surface roughness and gap width.
4	[14]	Standard GGG40 nodular cast iron	Regression analysis	Machining voltage discharge current, pulse duration, wire speed	Cutting rate, surface roughness	Cutting rate and surface roughness increases with increase in open circuit voltage, wire speed and discharge current.
5	[10]	SKDI1 alloy steel	Taguchi's L_{18} mixed orthogonal array, non-linear regression analysis	Pulse-on time, pulse-off time, table feed, wire speed, wire tension, flushing pressure	Gap width, MRR, SR, discharging frequency, gap voltage, normal discharge frequency ratio	Table feed and pulse-on time have significant influence on the MRR, gap voltage and discharge frequency. Gap width and surface roughness are mainly influenced by pulse-on time.
6	[8]	WC-Co composite	GRA along with Taguchi method	Pulse-on time, pulse-off time, taper angle, peak current, wire tension, dielectric flow rate	MRR, surface roughness	Taper angle, pulse-on time and pulse-off time are the most significant parameters affecting the MRR and surface roughness.
7	[20]	AISI 4140 steel (DIN 42CrMo4)	Regression analysis	Pulse duration, open circuit voltage, wire speed, dielectric fluid pressure	Wire wear ratio	Wire wear ratio increases with the increase in pulse duration and open circuit voltage. It decreases with increase in wire speed and dielectric fluid pressure.
8	[16]	Heat treated tool steel	Taguchi's L_{16} orthogonal array	Pulse-on time, wire tension, delay time, wire feed speed, ignition current intensity	MRR, surface roughness, wire wear ratio	Pulse-on time and ignition current had influenced more than the other parameters on MRR, SR and WW Ratio.
9	[13]	Hot die steel (40 mm thickness)	Taguchi's L_{16} orthogonal array, regression analysis, genetic algorithm	Pulse-on duration, pulse-off duration, current, bed speed, flushing rate	Dimensional error, surface roughness, volumetric material removal rate	High value of pulse-on results in higher MRR, better control on dimensional deviation and lower value of pulse-on results in better surface finish. Smaller pulse-off duration and flush rate gives better control on dimensional deviation
10	[7]	D2 tool steel	Taguchi's L_{18} orthogonal array, multiple and generic multiple linear regression models	Pulse-on time, pulse-off time, open voltage, wire feed velocity, wire tension, dielectric pressure, servo voltage, material thickness	MRR, Surface roughness, kerf	MRR increases and surface finish decreases with increase in pulse-on time, open voltage. MRR decreases with increase in servo voltage. Kerf increases with increase in open voltage, pulse-on time and wire tension.
11	[9]	Pure titanium (grade-2)	Box-Behnken design, RSM, desirability function	Pulse-on time, pulse-off time, peak current, wire tension, wire feed, spark gap voltage	Machining rate, dimensional deviation, surface roughness, wire wear ratio	Pulse-on time, pulse-off time and peak current are the major factors affecting MRR, WW ratio and dimensional deviation.

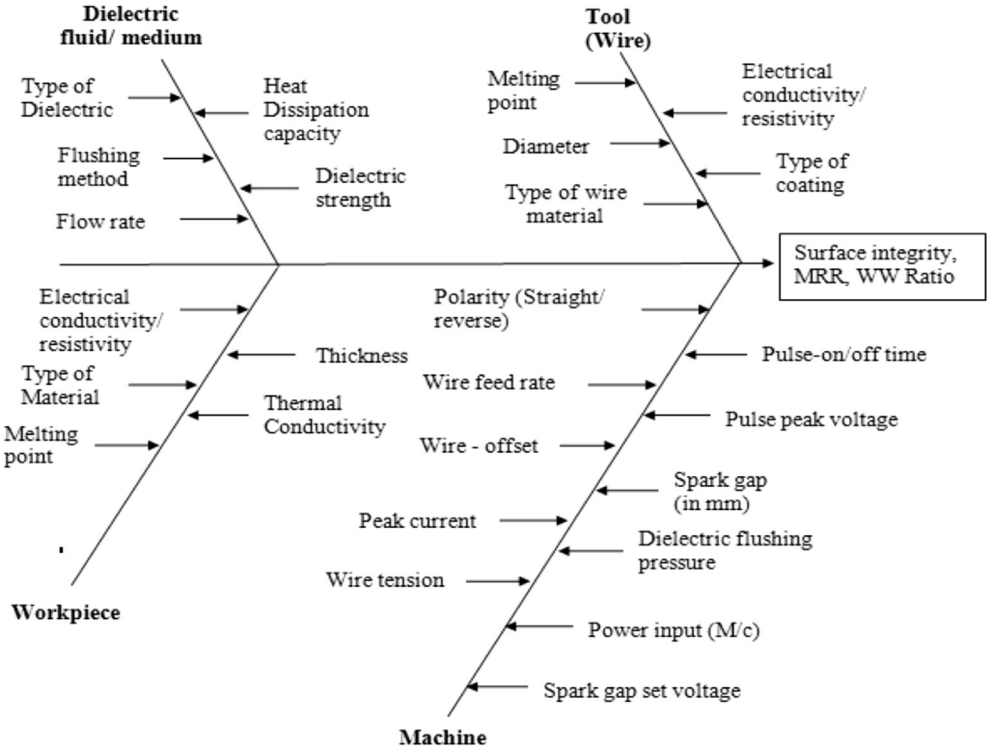

Fig. 2. Cause and effect diagram.

predicted mean has been applied. Three confirmation experiments for each performance characteristics have been performed at optimal settings of the process parameters and the average value has been reported.

For MRR,

The overall mean of the population is: $\mu = 0.04763$ g/min.

The predicted optimum value of MRR is calculated as,

$$\mu\text{MRR} = \left(\mu T_{\text{on}}3 + \mu T_{\text{off}}1 + \mu\text{IP}3 + \mu\text{WF}1 + \mu\text{WT}3 + \mu\text{SV}1\right) - (5\mu) = 0.1102 \text{ g/min}.$$

For calculation of CI_{CE}, Eq. (3) has been used [17].

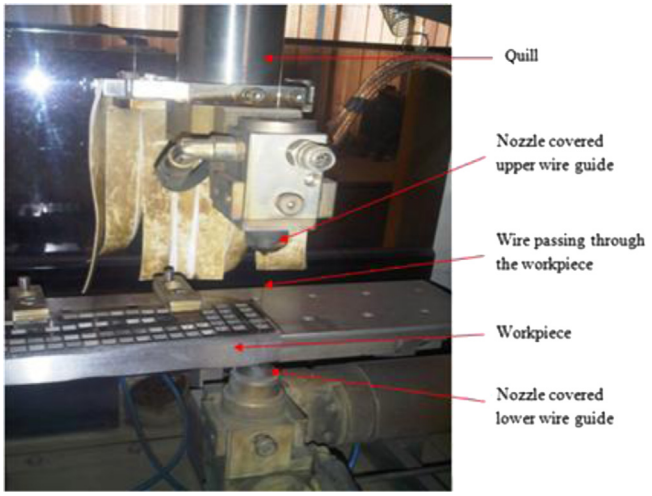

Fig. 3. Experimental setup of the WEDM.

$$\text{CI}_{\text{CE}} = \sqrt{F_{\alpha}(1 \cdot f_{\text{e}})\left\{\frac{1}{n_{\text{eff}}} + \frac{1}{R}\right\}V_{\text{e}}} \tag{3}$$

For MRR, $f_{\text{e}} = 56$,

$F_{\alpha}(1, f_{\text{e}}) = 4.02$

V_{e} = variance of error = 0.000018

$$n_{\text{eff}} = \frac{N}{1 + \text{Total DF involved in estimation of mean}} \tag{4}$$

N = total number of experiments

Hence $n_{\text{eff}} = 81/(1 + 12) = 6.231$

R = sample size = 3

Hence, putting all the values in Eq. (3)

$\text{CI}_{\text{CE}} = 0.00597$

The 95% confidence interval for μMRR is,

$\text{CI}_{\text{CE}} = 0.104 < \mu\text{MRR} < 0.116$

Similarly, for WWR,

The overall mean of the population is: $\mu = 0.087$

Table 2
Process parameters, symbols and their ranges.

Parameters designation	Process parameters	Level 1	Level 2	Level 3
A	T_{on} (pulse-on time)	106 μs	112 μs	118 μs
B	T_{off} (pulse-off time)	30 μs	42 μs	54 μs
C	IP (peak current)	80 A	120 A	160 A
D	Wire feed	6	8	10
E	Wire tension (g)	7 (1020)	9 (1260)	11 (1500)
F	SV (spark gap set voltage)	30 V	50 V	70 V
Constant parameters	Flushing pressure	01 (High)	01 (High)	01 (High)
	Servo feed	2050	2050	2050
	Pulse peak voltage	02	02	02

The predicted optimum value of WWR is calculated as,

$$\mu\text{WWR} = \left(\mu T_{\text{on}}1 + \mu T_{\text{off}}3 + \mu\text{IP1} + \mu\text{WF3} + \mu\text{WT1} + \mu\text{SV1}\right) - (5\mu)$$

$$= (0.08225 + 0.07907 + 0.08024 + 0.08558 + 0.08289 + 0.08320) - (5 \times 0.087) = 0.4932 - 0.4320$$

$\mu\text{WWR} = 0.0582$

V_e = variance of error = 0.0000309
$n_{\text{eff}} = 81/(1 + 12) = 6.231$
$\text{CI}_{\text{CE}} = 0.004$
The 95% confidence interval for μWWR is,
$\text{CI}_{\text{CE}} = 0.054 < \mu\text{WWR} < 0.062$

Table 7 shows the single response optimization results. Table 8 shows the confirmatory experimental results and values have been tabulated. Three experiments were conducted at the optimum settings of the process parameters for all the responses. The mean values of the responses from these experiments have been found to be well contained by the confidence intervals.

5. Multi-response optimization using grey relational analysis

5.1. Grey relational analysis

Grey relational analysis provides an efficient solution to the uncertainty, multi-input and discrete data problem. The relation between machining parameters and responses can be found out by using the GRA [6]. In order to optimize the MRR and WWR simultaneously using GRA, the following steps were followed:

Step 1: Calculate Mean (Data) for the corresponding responses using "Higher the better" type attribute for MRR and "Lower the better" type attribute for WWR.
Step 2: Normalize the data. Normalization is a transformation performed on a single data input to distribute the data evenly and scale it into an acceptable range for further analysis.
Step 3: Calculate the grey relational co-efficient for the normalized Mean (Raw data) values.
Step 4: Generate the grey relational grade.
Step 5: Perform ANOVA for identifying the significant factors and calculate the predicted optimum condition.

In the grey relational analysis, experimental results were first normalized and then the grey relational coefficient has been calculated from the normalized experimental data. Data pre-processing was performed on raw data (Mean data) for all experimental results (Table 9). Data pre-processing is a technique that involves transforming raw data into an understandable format. Raw data (Mean data) can be normalized by using the following expressions:

For MRR Higher the better (Eq. (5))

$$x_i^*(k) = \frac{x_i^0(k) - \min x_i^0(k)}{\max x_i^0(k) - \min x_i^0(k)} \tag{5}$$

For WWR, lower the better (Eq. (6))

$$x_i^*(k) = \frac{\max x_i^0(k) - x_i^0(k)}{\max x_i^0(k) - \min x_i^0(k)} \tag{6}$$

Table 3
L_{27} orthogonal array with parameters and interactions assigned to columns.

Run	A 1	B 2	A × B 3	A × B 4	C 5	A × C 6	A × C 7	B × C 8	D 9	E 10	B × C 11	F 12	13
1	1	1	1	1	1	1	1	1	1	1	1	1	1
2	1	1	1	1	2	2	2	2	2	2	2	2	2
3	1	1	1	1	3	3	3	3	3	3	3	3	3
4	1	2	2	2	1	1	1	2	2	2	3	3	3
5	1	2	2	2	2	2	2	3	3	3	1	1	1
6	1	2	2	2	3	3	3	1	1	1	2	2	2
7	1	3	3	3	1	1	1	3	3	3	2	2	2
8	1	3	3	3	2	2	2	1	1	1	3	3	3
9	1	3	3	3	3	3	3	2	2	2	1	1	1
10	2	1	2	3	1	2	3	1	2	3	1	2	3
11	2	1	2	3	2	3	1	2	3	1	2	3	1
12	2	1	2	3	3	1	2	3	1	2	3	1	2
13	2	2	3	1	1	2	3	2	3	1	3	1	2
14	2	2	3	1	2	3	1	3	1	2	1	2	3
15	2	2	3	1	3	1	2	1	2	3	2	3	1
16	2	3	1	2	1	2	3	3	1	2	2	3	1
17	2	3	1	2	2	3	1	1	2	3	3	1	2
18	2	3	1	2	3	1	2	2	3	1	1	2	3
19	3	1	3	2	1	3	2	1	3	2	1	3	2
20	3	1	3	2	2	1	3	2	1	3	2	1	3
21	3	1	3	2	3	2	1	3	2	1	3	2	1
22	3	2	1	3	1	3	2	2	1	3	3	2	1
23	3	2	1	3	2	1	3	3	2	1	1	3	2
24	3	2	1	3	3	2	1	1	3	2	2	1	3
25	3	3	2	1	1	3	2	3	2	1	2	1	3
26	3	3	2	1	2	1	3	1	3	2	3	2	1
27	3	3	2	1	3	2	1	2	1	3	1	3	2

where $x_i^*(k)$ is the sequence after the data processing; $x_i^0(k)$ is the original sequence of raw data (Mean data), $i = 1, 2, 3\ldots, m$ and $k = 1, 2, \ldots, n$ with $m = 27$ and $n = 2$; max $x_i^0(k)$ is the largest value of $x_i^0(k)$; min$x_i^0(k)$ is the smallest value of $x_i^0(k)$. Table 9 shows the normalized raw data (Mean data) for the MRR and WWR. The outcomes are denoted as $x_0^*(k)$ and $x_i^*(k)$ for reference sequence and comparability sequence, respectively.

5.2. Grey relational grade generation

The grey relational coefficient is calculated to express the relationship between the best (reference) and the actual raw data (Mean data). The grey relational coefficient is expressed as follows:

$$£_{ij}(k) = \frac{(\Delta)\min + \zeta(\Delta)\max}{(\Delta)\mathrm{oi}(k) + \zeta(\Delta)\max} \tag{7}$$

$$0 < £_{ij}(k) \leq 1$$

where, $\Delta_{oi}(k)$ is the deviation sequence of reference sequence

$$\Delta_{\min} = \min[\min \Delta_{oi}(k)]$$

$$\Delta_{\max} = \max[\max \Delta_{oi}(k)]$$

$£_{ij}$ The grey relational coefficient, ζ is is the distinguishing coefficient is set as 0.5 in this case. The deviation sequence (Δ)oi can be calculated as follow:

$$(\Delta\mathrm{MRR})01 = |1 - 0.175| = 0.825$$

$$(\Delta\mathrm{WWR})01 = |1 - 0.1838| = 0.8162$$

From the data in Table 9 we can find the following:

$$\Delta_{\max} = \Delta_{08}(\mathrm{MRR}) = \Delta_{13}(\mathrm{WWR}) = 1.000,$$

$$\Delta_{\min} = \Delta_{20}(\mathrm{MRR}) = \Delta_{22}(\mathrm{WWR}) = 0.000,$$

The grey relational coefficient is calculated from the Eq. (7) (Table 9). For example:

$$£_{1(\mathrm{MRR})} = [0.000 + (0.5 \times 1.000)]/[0.825 + (0.5 \times 1.000)] = 0.3774$$

$$£_{1(\mathrm{WWR})} = [0.000 + (0.5 \times 1.000)]/[0.8168 + (0.5 \times 1.000)] = 0.3799$$

The grey relational grade Y_j can be obtained as:

$$Y_j = \frac{1}{m}\sum_{i=1}^{m} £ \tag{8}$$

Where Y_j the grey relational grade for the jth experiment and m is the number of performance characteristics. The higher grey relational grade implies the better product quality. By assigning equal weighting values of MRR = 0.5 and WWR = 0.5, GR grade is calculated (Table 9).

6. Results and discussions

Increasing the pulse-on time and peak current increases the material removal rate as with the increase in pulse-on time and peak current, number of electrons striking the work surface in a single discharge increases thus eroding out more material from the

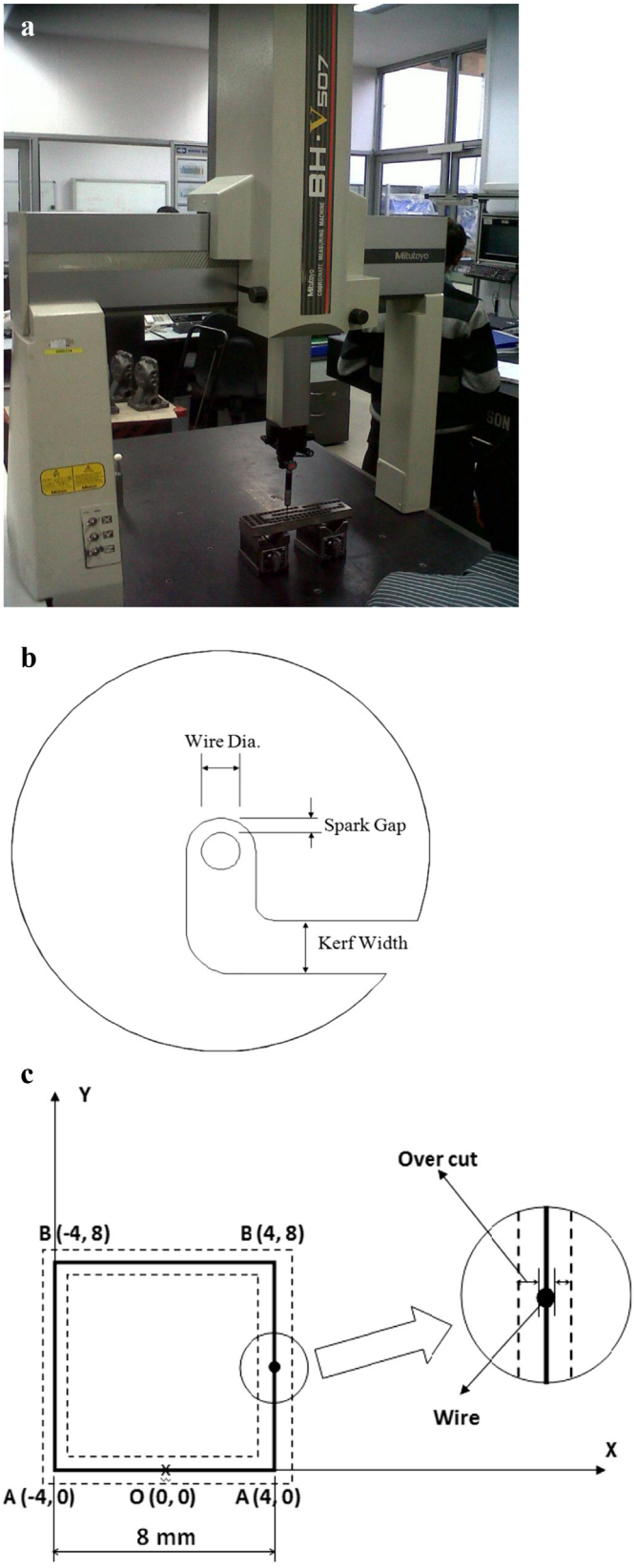

Fig. 4. a. CMM measuring kerf of the machined workpiece. b. Kerf width. c. Machining profile of the workpiece.

Table 4
Experimental data of material removal rate and wire wear ratio.

Sr. no.	MRR 1	MRR 2	MRR 3	*S/N* ratio	Mean	WWR 1	WWR 2	WWR 3	*S/N* ratio	Mean
1	0.0321	0.0320	0.0334	−29.7736	0.0325	0.071	0.068	0.065	23.3442	0.0680
2	0.0377	0.0363	0.0366	−28.6708	0.0369	0.112	0.107	0.109	19.2234	0.1093
3	0.0350	0.0362	0.0375	−28.8310	0.0362	0.102	0.104	0.107	19.6299	0.1043
4	0.0191	0.0190	0.0197	−34.3131	0.0193	0.077	0.081	0.079	22.0456	0.0790
5	0.0315	0.0302	0.0313	−30.1755	0.0310	0.081	0.084	0.085	21.5818	0.0833
6	0.0299	0.0312	0.0323	−30.1412	0.0312	0.078	0.076	0.073	22.4187	0.0757
7	0.0138	0.0152	0.0167	−36.4165	0.0152	0.065	0.062	0.068	23.7454	0.0649
8	0.0128	0.0129	0.0137	−37.6430	0.0131	0.082	0.083	0.079	21.7927	0.0813
9	0.0179	0.0164	0.0170	−35.3545	0.0171	0.076	0.073	0.074	22.5751	0.0743
10	0.0617	0.0586	0.0594	−24.4565	0.0599	0.089	0.085	0.091	21.0653	0.0884
11	0.0517	0.0508	0.0504	−25.8554	0.0510	0.112	0.117	0.119	18.7080	0.1160
12	0.0705	0.0715	0.0735	−22.8778	0.0718	0.098	0.095	0.093	20.4011	0.0955
13	0.0541	0.0494	0.0531	−25.6682	0.0522	0.052	0.049	0.051	25.8976	0.0507
14	0.0504	0.0487	0.0503	−26.0578	0.0498	0.093	0.095	0.092	20.5985	0.0933
15	0.0339	0.0344	0.0354	−29.2363	0.0345	0.082	0.078	0.081	21.9001	0.0803
16	0.0166	0.0152	0.0195	−35.4749	0.0171	0.065	0.069	0.076	23.0798	0.0700
17	0.0313	0.0296	0.0304	−30.3422	0.0304	0.105	0.100	0.103	19.7697	0.1027
18	0.0260	0.0268	0.0277	−31.4379	0.0268	0.089	0.091	0.093	20.8178	0.0910
19	0.0723	0.0734	0.0725	−22.7650	0.0727	0.078	0.073	0.075	22.4637	0.0753
20	0.1278	0.1189	0.1242	−18.1672	0.1237	0.086	0.087	0.091	21.1077	0.0880
21	0.1061	0.1137	0.1098	−19.1944	0.1099	0.094	0.092	0.089	20.7536	0.0917
22	0.0812	0.0835	0.0839	−21.6329	0.0829	0.145	0.147	0.143	16.7810	0.1448
23	0.0575	0.0565	0.0545	−25.0211	0.0561	0.093	0.091	0.088	20.8488	0.0907
24	0.0987	0.1032	0.1033	−19.8567	0.1017	0.108	0.102	0.106	19.5499	0.1053
25	0.0391	0.0382	0.0408	−28.1096	0.0394	0.079	0.081	0.083	21.8285	0.0810
26	0.0341	0.0352	0.0361	−29.0930	0.0351	0.082	0.079	0.077	22.0080	0.0793
27	0.0388	0.0379	0.0390	−28.2738	0.0386	0.067	0.069	0.065	23.4759	0.0670

work surface per discharge. Similarly, MRR decreases with an increased pulse-off time and spark gap set voltage for a constant pulse-on time and peak current. Overall machining time increases with increase in pulse-off time (T_{off}) as the discharge frequency decreases with increase in pulse-off time. Long pulse-off time leads to drop in the temperature of the workpiece before the next spark starts and therefore MRR decreases. High peak current results in high discharge frequency, hence results in high MRR. Machining speed increases with decrease in spark gap set voltage value. Decreasing spark gap set voltage closes the spark gap which results in rapid and large ionisation of dielectric fluid which gives rise to more melting of work material and hence more MRR. Increasing wire tension leads to the easy and rapid escape of eroded material out of the spark gap and increases MRR. Fig. 5 shows the main effects plot for material removal rate and wire wear ratio versus pulse-on time (T_{on}), pulse-off time (T_{off}), peak current (IP), wire feed (WF), wire tension (WT) and spark gap set voltage (SV). According to these figures, the material removal rate increased when the pulse-on time (T_{on}), peak current and wire tension were increased. Pulse-on time (T_{on}) is found to be the major factor (Table 5) affecting the MRR (46.09%). The percent contribution of pulse-off time (T_{off}), peak current and spark gap set voltage on the MRR are 32.97, 1.45 and 6.68% respectively. High pulse-on time (T_{on}) results in faster erosion of the material as longer duration of spark results in higher spark energy release hence increase in material removal

Table 5
Analysis of variance (mean value) for MRR (g/min).

Source	DF	Seq SS	Adj MS	*F*	*P*	%Age contribution
T_{on}	2	0.0310911	0.0155455	865.15	0.000	46.09
T_{off}	2	0.0222424	0.0111212	618.93	0.000	32.97
IP	2	0.0009814	0.0004907	27.31	0.000	1.45
WF	2	0.0005672	0.0002836	15.78	0.000	0.84
WT	2	0.0002972	0.0001486	8.27	0.001	0.44
SV	2	0.0045043	0.0022521	125.34	0.000	6.68
T_{on} * T_{off}	4	0.0048007	0.0012002	66.79	0.000	7.12
T_{on} * IP	4	0.0007602	0.00019	10.58	0.000	1.13
T_{off} * IP	4	0.0012048	0.0003012	16.76	0.000	1.79
Error	56	0.0010062	0.000018			1.49
Total	80	0.0674555				
S = 0.00423894	R-Sq = 98.51%		R-Sq (adj) = 97.87%			

Table 6
Analysis of variance (mean value) for WWR.

Source	DF	Seq SS	Adj MS	*F*	*P*	%Age contribution
T_{on}	2	0.001152	0.000576	18.66	0.000	4.09
T_{off}	2	0.0027889	0.0013944	45.18	0.000	9.9
IP	2	0.0024748	0.0012374	40.09	0.000	8.79
WF	2	0.0001236	0.0000618	2	0.145	0.43
WT	2	0.0010124	0.0005062	16.4	0.000	3.59
SV	2	0.0015384	0.0007692	24.92	0.000	5.46
T_{on} * T_{off}	4	0.0090486	0.0022621	73.29	0.000	32.13
T_{on} * IP	4	0.0059487	0.0014872	48.18	0.000	21.12
T_{off} * IP	4	0.0023444	0.0005861	18.99	0.000	8.32
Error	56	0.0017285	0.0000309			6.13
Total	80	0.0281603				
S = 0.0055556	R-Sq = 93.86%		R-Sq (adj) = 91.23%			

Table 7
Single response optimisation results.

Method	Characteristics	Optimal condition	Optimal predicted value
Single response optimisation	Material removal rate	T_{on}3 T_{off}1 IP3 WF1 WT3 SV1	0.1102 g/min
	Wire wear ratio	T_{on}1 T_{off}3 IP1 WF3 WT1 SV1	0.058

Table 8
Confirmatory experimental results.

Response (units)	Predicted value	Experimental value	CI_{CE}
MRR (g/min)	0.1102	0.1159	0.104 < μMRR < 0.116
Wire wear ratio	0.058	0.061	0.054 < μWWR < 0.062

Table 9
Grey relational grade data.

Sr. no.	Mean (MRR) normalized	Mean (WWR) normalized	Δ_{MRR}	Δ_{WWR}	GR coeff. (MRR)	GR coeff. (WWR)	GR Grade	GR grade *S*/*N* ratio	GR grade mean
1	0.175	0.1838	0.825	0.8162	0.3774	0.3799	0.5543	−5.1251	0.5543
2	0.2147	0.6228	0.7853	0.3772	0.389	0.57	0.4172	−7.5937	0.4172
3	0.2089	0.5697	0.7911	0.4303	0.3873	0.5374	0.4273	−7.3844	0.4273
4	0.0554	0.3006	0.9446	0.6994	0.3461	0.4169	0.4853	−6.2795	0.4853
5	0.1617	0.3466	0.8383	0.6534	0.3736	0.4335	0.4821	−6.3374	0.4821
6	0.1631	0.2652	0.8369	0.7348	0.374	0.4049	0.5137	−5.7857	0.5137
7	0.0191	0.1511	0.9809	0.8489	0.3376	0.3707	0.5528	−5.1489	0.5528
8	0	0.3254	1	0.6746	0.3333	0.4257	0.4696	−6.5663	0.4696
9	0.0359	0.251	0.9641	0.749	0.3415	0.4003	0.5036	−5.9578	0.5036
10	0.4232	0.4007	0.5768	0.5993	0.4643	0.4548	0.5097	−5.8529	0.5097
11	0.3423	0.6936	0.6577	0.3064	0.4319	0.62	0.4254	−7.4240	0.4254
12	0.5311	0.4755	0.4689	0.5245	0.516	0.4881	0.5143	−5.7758	0.5143
13	0.3534	0	0.6466	1	0.4361	0.3333	0.7180	−2.8771	0.7180
14	0.3318	0.4528	0.6682	0.5472	0.428	0.4775	0.4764	−6.4410	0.4764
15	0.1937	0.3148	0.8063	0.6852	0.3828	0.4219	0.4982	−6.0516	0.4982
16	0.036	0.205	0.964	0.795	0.3415	0.3861	0.5254	−5.5909	0.5254
17	0.1564	0.552	0.8436	0.448	0.3721	0.5274	0.4237	−7.4584	0.4237
18	0.1239	0.4281	0.8761	0.5719	0.3633	0.4664	0.4511	−6.9155	0.4511
19	0.5393	0.261	0.4607	0.739	0.5205	0.4036	0.5887	−4.6017	0.5887
20	1	0.3962	0	0.6038	1	0.453	0.7790	−2.1697	0.7790
21	0.8751	0.4351	0.1249	0.5649	0.8002	0.4695	0.6674	−3.5121	0.6674
22	0.6311	1	0.3689	0	0.5755	1	0.4544	−6.8513	0.4544
23	0.3891	0.4245	0.6109	0.5755	0.4501	0.4649	0.4955	−6.0999	0.4955
24	0.8016	0.5798	0.1984	0.4202	0.716	0.5434	0.5895	−4.5904	0.5895
25	0.2372	0.3219	0.7628	0.6781	0.396	0.4244	0.5022	−5.9830	0.5022
26	0.199	0.3041	0.801	0.6959	0.3843	0.4181	0.5031	−5.9677	0.5031
27	0.2303	0.1732	0.7697	0.8268	0.3938	0.3768	0.5683	−4.9088	0.5683

rate [16]. Table 6 shows the ANOVA results of wire wear ratio. According to Table 6, peak current (IP) and pulse-off time are found to be the major factors affecting the wire wear ratio. The interaction between pulse-on time (T_{on}) and pulse-off time (T_{off}) was found to be highly significant (32.13%). Results show that, increasing the pulse duration increases the WWR, whereas increasing the wire speed decreases the WWR which is in agreement with the findings of Tosun and Cogun [20] and Kumar et al. [9]. Decreasing WWR with increasing wire speed can be explained by fewer craters being formed per unit length of the wire electrode. Table 10 shows the comparison of results between single response optimisation and multi response optimisation using grey relational analysis. The standardized residuals are plotted on a normality plot to check the departure of the data from normality. Fig. 6 shows the Main Effects plot of Data means for GR Grade (MRR and WWR). Fig. 7 (Residual plots for MRR) and Fig. 8 (Residual plots for WWR) shows that the residuals are almost falling on a straight line, which indicates that the residuals are normally distributed and the normality assumption is valid. The adequacies of the ANOVA model are also tested through the correlation between calculated and experimental values which is shown in scattered plot, residual vs. fitted values. Moreover, the standardized residuals are exhibiting a random, irregular pattern, as observed in the residual vs. order plot. This validates that the experimental data has been obtained on

Table 10
Comparison of results.

Method	Characteristics	Optimal condition	Optimal experimental value
Single response optimisation (Taguchi method)	Material removal rate	T_{on}3 T_{off}1 IP3 WF1 WT3 SV1	0.1159 g/min
	Wire wear ratio	T_{on}1 T_{off}3 IP1 WF3 WT1 SV1	0.061
Multi response optimisation (GRA)	Material removal rate	T_{on}3 T_{off}1 IP1 WF1 WT1 SV1	0.114 g/min
	Wire wear ratio		0.082

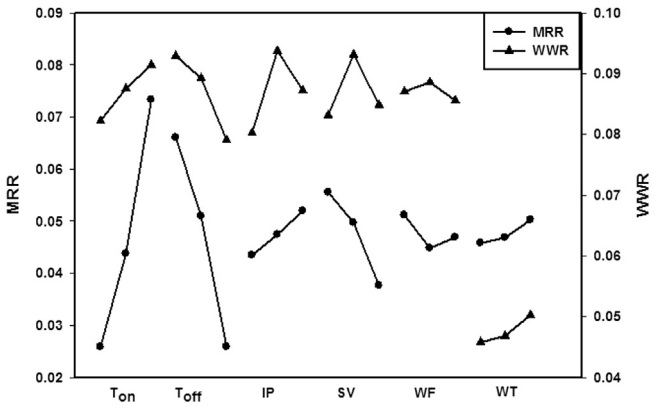

Fig. 5. Main effects plot of data means for MRR and WWR.

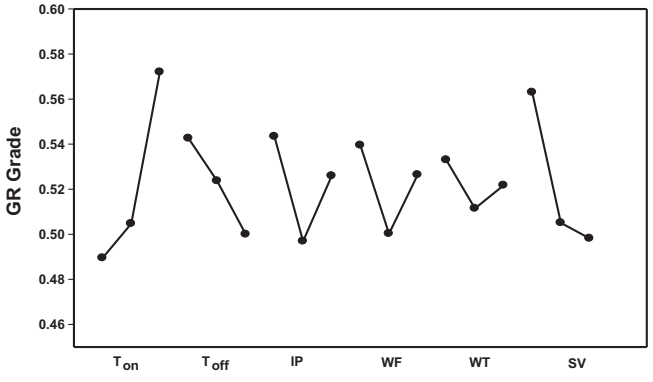

Fig. 6. Main effects plot of data means for GR grade (MRR and WWR).

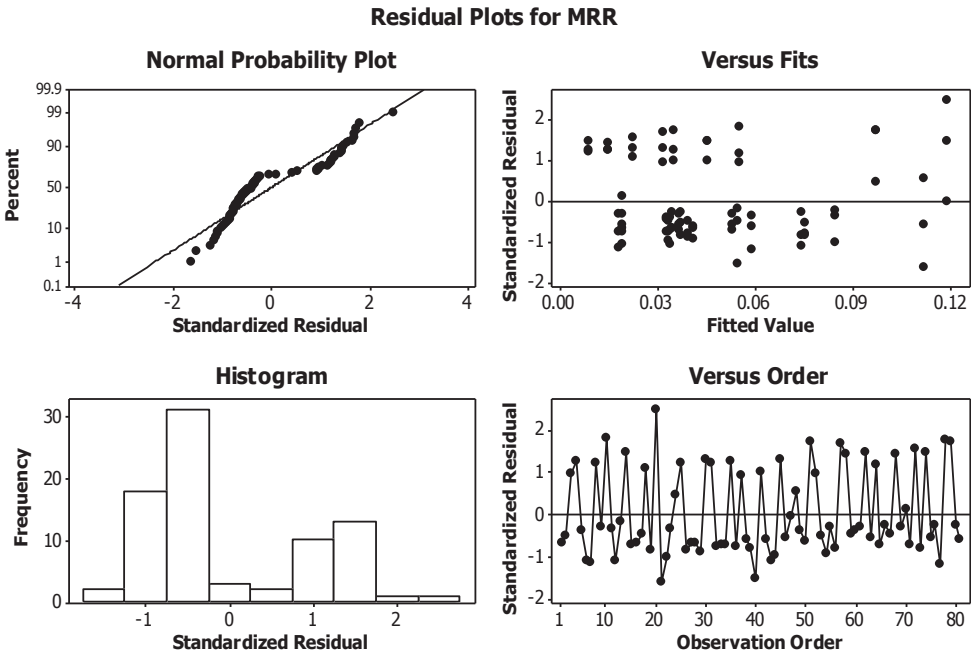

Fig. 7. Residual plots for MRR.

purely random basis and there is no specific trend in the residual data, which further validates the independence of the data. The model assumptions have been tested for both the responses and have been found to be valid.

6.1. Scanned electron microscopy (SEM) of the machined samples

The investigation of the microstructure of machined work surface was performed for assessment of the surface quality obtained using WEDM process. The Specimens were observed with scanning electron microscope Hitachi S-3400N with an accelerating voltage of 10.0 kV. Etching of the specimens was done in a mixture composed of 50 ml HCl, 50 ml distilled water and 5 g copper sulphate for 1 min. The two specimens were selected for microstructure observation with low value of MRR and another with high value of MRR. The microstructures of these samples have been depicted in Fig. 9a and b. Fig. 9a and b shows the microstructure of the machined sample at Experiment no. 7, Table 3 (T_{on}: 106 μs, T_{off}: 54 μs, IP: 80 A, SV: 50 V, WF: 10 and WT: 11) and microstructure of the machined sample at Experiment no. 20, Table 3 (T_{on}: 118 μs, T_{off}: 30 μs, IP: 120 A, SV: 30 V, WF: 6 and WT: 11) respectively. In case of high MRR (Exp. No. 20, Table 4), pulse-on time is set at its highest

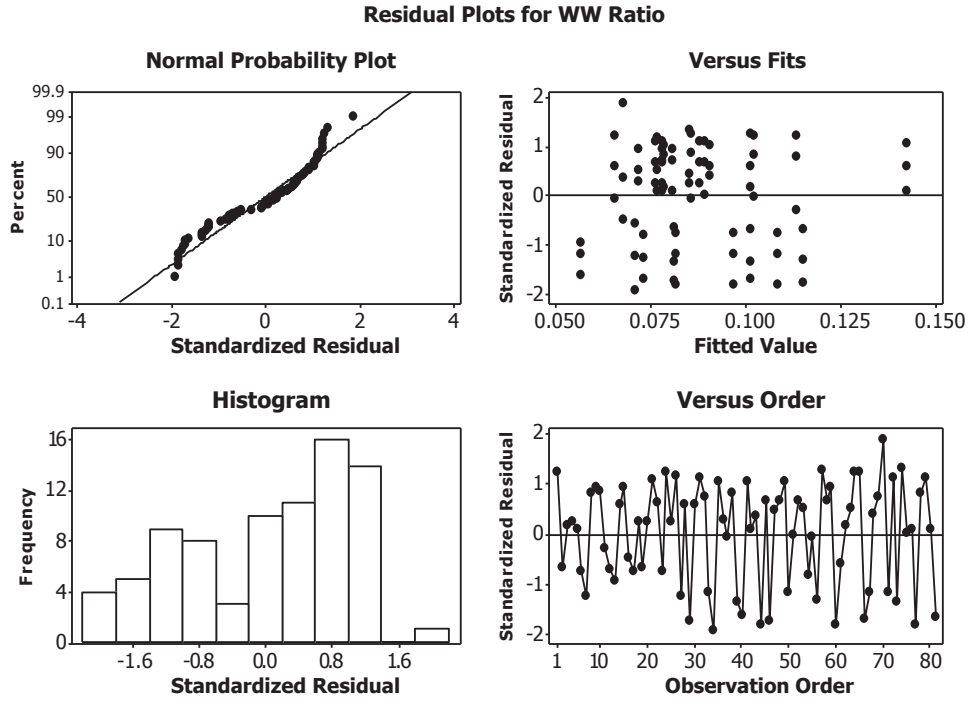

Fig. 8. Residual plots for WWR.

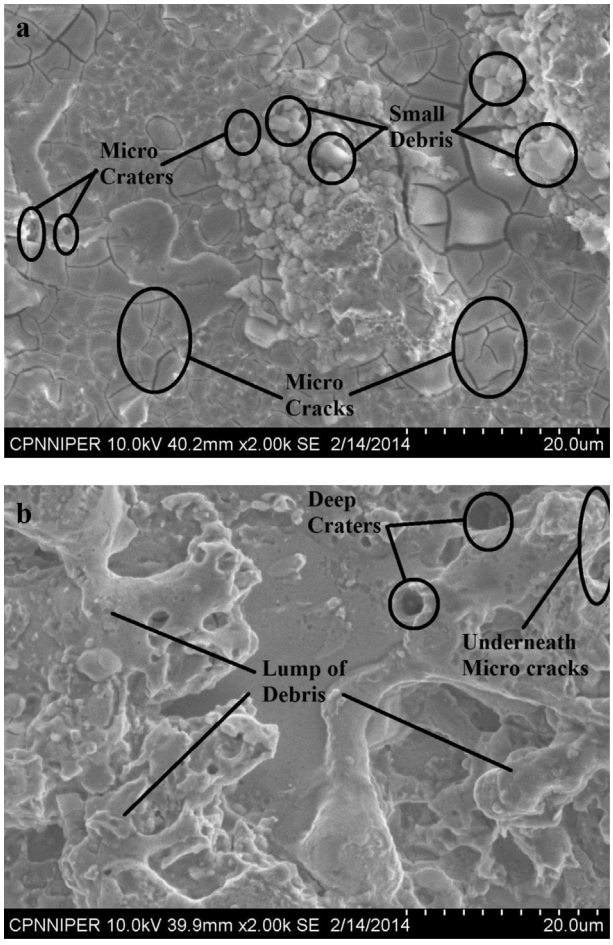

Fig. 9. a. Microstructure of the machined sample at experiment no. 7, Table 3 (T_{on}: 106 μs, T_{off}: 54 μs, IP: 80 A, SV: 50 V, WF: 10 and WT: 11). b. Microstructure of the machined sample at experiment no. 20, Table 3 (T_{on}: 118 μs, T_{off}: 30 μs, IP: 120 A, SV: 30 V, WF: 6 and WT: 11).

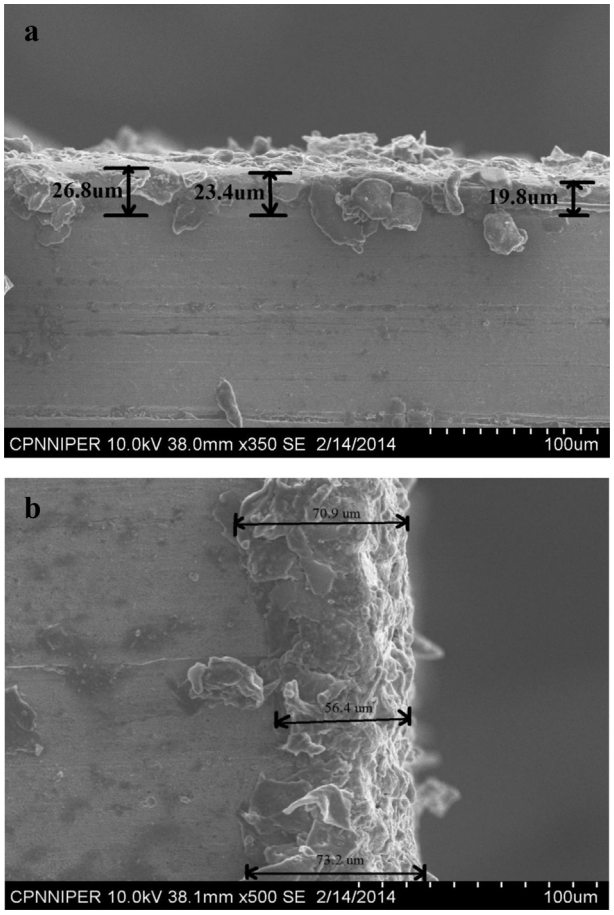

Fig. 10. a. Recast layer of the machined sample at experiment no. 7, Table 3 (T_{on}: 106 μs, T_{off}: 54 μs, IP: 80 A, SV: 50 V, WF: 10 and WT: 11). b. Recast layer of the machined sample at experiment no. 20, Table 3 (T_{on}: 118 μs, T_{off}: 30 μs, IP: 120 A, SV: 30 V, WF: 6 and WT: 11).

level, pulse-off time being at lowest level, while peak current has intermediate level. This can be observed (Fig. 9b) that the high value of applied erosive power caused the formation of large debris and deep holes/craters as apparent on the surface. These may be the places where individual discharges were able to penetrate far into the workpiece. It is possible that a high energy pulse vaporizes a large amount of metal on the initial discharge. Smaller current discharges might only remove a small amount of metal initially, but a larger percentage is heated to the melting stage and gets redeposit back on the surface as recast layer. The higher pulse-on time increases the metal removal rate and also results in accelerated depletion of brass wire; the residual particle of brass wire get adhered on the cutting surface. This generates a larger built-up layer. The other sample was machined at experimental condition corresponding to low energy input rate (Exp. No. 7, Table 4), where the parameters such as pulse-on time and peak current are set at their lowest values (level 1). The machined surface in this case (Fig. 9a) appears to be smoother as discharge craters are extremely small with small amount of debris.

6.2. Recast layer

During machining of the workpiece, spark melts a small portion of the workpiece and wire electrode. A portion of this molten material is ejected and flushed away. The remaining material resolidifies to form a surface layer known as the recast layer. Recast layer thickness tends to increase with increased current pulse duration and increased energy per spark. Recast layer thickness increases with decreasing pulse-off time. The depth of this top melted zone depends on the pulse energy and duration. A higher pulse-on time setting leads to thicker recast layer. This indicates that recast layer thickness increases with an increasing peak discharge current, pulse-on time and energy per spark and with decreasing pulse-off time. Fig. 10a and b shows the recast layer of the machined sample at experiment no. 7, Table 3 (T_{on}: 106 μs, T_{off}: 54 μs, IP: 80 A, SV: 50 V, WF: 10 and WT: 11) and Recast layer of the machined sample at experiment no. 20, Table 3 (T_{on}: 118 μs, T_{off}: 30 μs, IP: 120 A, SV: 30 V, WF: 6 and WT: 11) respectively. Fig. 10b shows that with greater energy release in each spark, the quantity of workpiece material which is melted is greater, resulting in a larger quantity of molten material which resolidifies to form the recast layer. Fig. 10b shows that the recast layer is more than double as compared to Fig. 10a.

6.3. EDS analysis

Energy dispersive spectrometry (EDS) is used for structural and compositional analysis. In this, the specimen to be analysed is bombarded with electrons which results in emission of characteristic X-rays. These X-rays can be measured using energy dispersive spectrometry (EDS). The constituents of the modified surface layers after WEDM have been analysed by EDS analysis in which the weight percentage of elements is calculated over a very small area

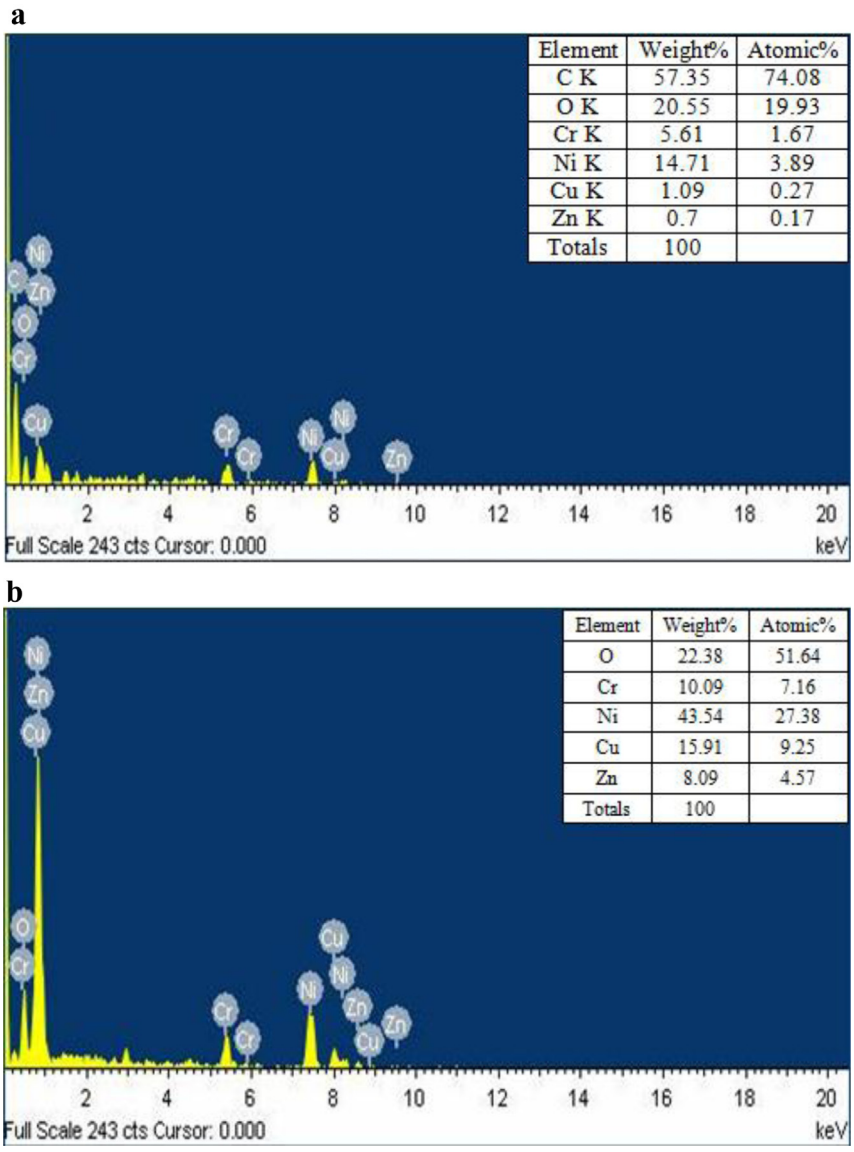

Fig. 11. a. Spectra of EDS of the machined sample at experiment no. 7, Table 3 (T_{on}: 106 μs, T_{off}: 54 μs, IP: 80 A, SV: 50 V, WF: 10 and WT: 11). b. Spectra of EDS of the machined sample at experiment no. 20, Table 3 (T_{on}: 118 μs, T_{off}: 30 μs, IP: 120 A, SV: 30 V, WF: 6 and WT: 11).

of the surface. Fig. 11a and b shows the spectra of EDS of the machined sample at experiment no. 7, Table 3 (T_{on}: 106 μs, T_{off}: 54 μs, IP: 80 A, SV: 50 V, WF: 10 and WT: 11) and spectra of EDS of the machined sample at experiment no. 20, Table 3 (T_{on}: 118 μs, T_{off}: 30 μs, IP: 120 A, SV: 30 V, WF: 6 and WT: 11) respectively. Fig. 11a and b clearly indicate the presence of copper and zinc in the workpieces. Since the Nimonic 80A does not contains zinc and the machined sample (Fig. 11b) contains 15.91% copper and 8.09% zinc, which shows that these elements migrated into the workpiece from the wire electrode during machining. The machined workpiece (Fig. 11a) contains 1.09% copper and 0.7% zinc only, which shows that on lower value of pulse-on time and higher value of pulse-off time, the wire deposition on the machined surface is low.

7. Conclusion

In this study, the effect of machining parameters on the machining outputs (material removal rate and wire wear ratio) of Nimonic 80A was investigated experimentally in WEDM.

1. Pulse-on time (T_{on}) and pulse-off time (T_{off}) have been found to be the most significant factors for MRR at 95% significance level, with percent contributions of 46% and 33% respectively. Other factors and two factor interactions investigated have also been found to be significant for MRR as response, however, their contribution in the variation of MRR is relatively much less.
2. All of the input parameters investigated in the study have been found to be statistically significant for wire wear ratio. The two factor interactions ($T_{on} \times T_{off}$ and $T_{on} \times$ IP) have been found to contribute most to the variation in WWR.
3. Multi-response optimization of the two responses investigated has yielded a composite optimal setting as $T_{on}3$ $T_{off}1$ IP1 WF1 WT1 SV1 which has been validated through confirmation experiments.
4. The higher discharge energy results in melting expulsion, leading to the formation of a deeper and larger crater on the surface of the workpiece as observed in the microstructures.
5. The recast layer has been observed to increase with increase in pulse-on time and peak current. Recast layer observed on the

machined surface has been found to be almost 100% thicker for the sample machined at high discharge energy level when compared to the sample machined at low discharge energy level.

References

[1] D.F. Dauw, L. Albert, About the evolution of tool wears performance in wire EDM, Ann. CIRP 41 (1) (1992) 221–225.

[2] E.O. Ezugwu, Key improvements in the machining of difficult-to-cut aerospace alloys, Int. J. Mach. Tools Manuf. 45 (2005) 1353–1367.

[3] E.O. Ezugwu, J. Bonney, Y. Yamane, An overview of the machinability of aeroengine alloys, J. Mater. Process. Technol. 134 (2003) 233–253.

[4] E.O. Ezugwu, Z.M. Wang, A.R. Machado, The machinability of nickel-based alloys: a review, J. Mater. Process. Technol. 86 (1999) 01–16.

[5] El-Hofy Hassan, Advanced Machining Processes, McGraw-Hill Publishing Company Limited, New York, USA, 2003.

[6] J.T. Huang, Y.S. Liao, Optimization of machining parameter of wire-EDM based on grey relational and statistical analyses, Int. J. Prod. Res. 41 (8) (2003) 1707–1720.

[7] A. Ikram, N.A. Mufti, M.Q. Saleem, A.R. Khan, Parametric optimization for surface roughness, kerf and MRR in wire electrical discharge machining (WEDM) using Taguchi design of experiment, J. Mech. Sci. Technol. 27 (7) (2013) 2133–2141, http://dx.doi.org/10.1007/s12206-013-0526-8.

[8] K. Jangra, S. Grover, A. Aggarwal, Simultaneous optimization of material removal rate and surface roughness for WEDM of WCCo composite using grey relational analysis along with Taguchi method, Int. J. Ind. Eng. Comput. 2 (2011) 479–490.

[9] A. Kumar, V. Kumar, J. Kumar, Multiresponse optimization of process parameters based on response surface methodology for pure titanium using WEDM process, Int. J. Adv. Manuf. Technol. (2013), http://dx.doi.org/10.1007/s00170-013-4861-9.

[10] Y.S. Liao, J.T. Huang, H.C. Su, A study on the machining-parameters optimization of wire electrical discharge machining, J. Mater. Process. Technol. 71 (1997) 487–493.

[11] S.S. Mahapatra, A. Patnaik, Optimization of wire electrical discharge machining (WEDM) process parameters using Taguchi method, Int. J. Adv. Manuf. Technol. 34 (2007) 911–925.

[12] S.S. Mahapatra, A. Patnaik, Parametric optimization of wire electrical discharge machining (WEDM) process using taguchi method, J. Braz. Soc. Mech. Sci. Eng. 28 (2006) 422–429.

[13] K. Nixon, H.V. Ravindra, Parametric influence and optimization of wire EDM of hot die steel, Mach. Sci. Technol. Int. J. 15 (1) (2011) 47–75, http://dx.doi.org/10.1080/10910344.2011.557966.

[14] N. Ozdemir, C. Ozek, An investigation on machinability of nodular cast iron by WEDM, Int. J. Manuf. Technol. 28 (2006) 869–872.

[15] J. Prohaszka, A.G. Mamalis, N.M. Vaxevanidis, The effect of electrode material on machinability in wire electro-discharge machining, J. Mater. Process. Technol. 69 (1997) 233–237.

[16] R. Ramakrishnan, L. Karunamoorthy, Multi response optimization of wire EDM operations using robust design of experiments, Int. J. Adv. Manuf. Technol. 29 (2006) 105–112, http://dx.doi.org/10.1007/s00170-004-2496-6.

[17] P.J. Ross, Taguchi Techniques for Quality Engineering, second ed., Tata McGraw-Hill Publishing Company Limited, New Delhi, 2005.

[18] D. Scott, S. Bovina, K.P. Rajkumar, Analysis and optimization of parameter combinations in wire electrical discharge machining, Int. J. Prod. Res. 29 (11) (1991) 2189–2207.

[19] T.A. Spedding, Z.Q. Wang, Study on modelling of wire EDM process, J. Mater. Process. Technol. 69 (1997) 18–28.

[20] N. Tosun, C. Cogun, An investigation on wire wear in WEDM, J. Mater. Process. Technol. 134 (2003) 273–278.